POLITECNICO DI TORINO
Repository ISTITUZIONALE

Physics design of current drive and strategy of heating system for EHL-2 spherical torus

Original
Physics design of current drive and strategy of heating system for EHL-2 spherical torus / JIANG , X.., SHI , Y.., SONG , S.., LIU , W.., YANG , G.., SONG , X.., WANG , X.., GU , X.., YIN , G.., YANG , D.., ZHAO , H.., WANG , Y.., XIE , H.., LI , P.., WANG , H.., ZHANG , K.., HAN , L.., WU , X.., LIU , C.., WU , B.., et al.. - In: PLASMA SCIENCE & TECHNOLOGY. - ISSN 1009-0630. - 27:2(2025), pp. 1-14. [10.1088/2058-6272/adae71]

Availability:
This version is available at: 11583/3009148 since: 2026-03-24T14:27:23Z

Publisher:
IOP Publishing

Published
DOI:10.1088/2058-6272/adae71

Terms of use:

This article is made available under terms and conditions as specified in the corresponding bibliographic description in the repository

Publisher copyright
ACS preprint/submitted version

This document is the unedited Author's version of a Submitted Work that was subsequently accepted for publication in PLASMA SCIENCE & TECHNOLOGY, copyright © American Chemical Society after peer review. To access the final edited and published work see https://iopscience.iop.org/article/10.1088/2058-6272/adae71 / http://dx.doi.org/10.1088/2058-6272/adae71.

(Article begins on next page)

08 November 2026

Physics design of current drive and strategy of heating system for EHL-2 spherical torus

Xinchen JIANG (姜欣辰)[1,2,3], Yuejiang SHI (石跃江)[2,3,*], Shaodong SONG (宋绍栋)[2,3], Wenjun LIU (刘文军)[2,3], Guang YANG (杨光)[2,3], Xianming SONG (宋显明)[2,3], Xueyun WANG (王雪韵)[2,3], Xiang GU (顾翔)[2,3], Gang YIN (尹刚)[2,3], Danke YANG (杨丹可)[2,3], Hanyue ZHAO (赵寒月)[2,3], Yumin WANG (王嵎民)[2,3], Huasheng XIE (谢华生)[2,3], Pengmin LI (李鹏敏)[2,3], Hanqing WANG (王汉清)[2,3], Keqing ZHANG (张克卿)[2,3], Lei HAN (韩磊)[2,3], Xiaohe WU (邬潇河)[4], Chengyue LIU (刘成岳)[5], Bin WU (吴斌)[6], Chengyi SONG (宋城邑)[7], Chunyan LI (李春艳)[7], Jiakang CHEN (陈嘉康)[8], Pingwei ZHENG (郑平卫)[7,8], D Banerjee[9], Qingwei YANG (杨青巍)[10], Jiaqi DONG (董家齐)[10], Yunfeng LIANG (梁云峰)[2,11], Baoshan YUAN (袁保山)[2,3], Yueng-Kay Martin PENG (彭元凯)[2,3], Xianmei ZHANG (张先梅)[1,*], and the EHL-2 Team[2,3]

[1]School of Physics, East China University of Science and Technology, Shanghai 200237, People's Republic of China

[2]Hebei Key Laboratory of Compact Fusion, Langfang 065001, People's Republic of China

[3]ENN Science and Technology Development Co., Ltd., Langfang 065001, People's Republic of China

[4]University of Science and Technology of China, Hefei 230026, People's Republic of China

[5]School of Physics, Hefei University of Technology, Hefei 230009, People's Republic of China

[6]Institute of Plasma Physics, Chinese Academy of Science, Hefei 230026, People's Republic of China

[7]School of Nuclear Science and Technology, University of South China, Hengyang 421001, People's Republic of China

[8]School of Resource Environment and Safety Engineering, University of South China, Hengyang 421001, People's Republic of China

[9]DISAT, Polytechnic University of Turin, Torino 10129, Italy

[10]Southwestern Institute of Physics, Chengdu 610225, People's Republic of China

[11]Forschungszentrum Jülich GmbH, Institute of Fusion Energy and Nuclear Waste Management - Plasmaphysik, Jülich 52425, Germany

[*]E-mail of corresponding authors: yjshi@ipp.ac.cn and zhangxm@ecust.edu.cn

Abstract

ENN He Long-2 (EHL-2) is the next-generation large mega-Ampere (MA) spherical torus (ST) proposed and funded by ENN company. The design parameters are: T_{i0} > 30 keV, $n_{e0} \sim 1 \times 10^{20}$ m^{-3}, I_p ~ 3 MA, B_t ~ 3 T. How to achieve several MA current flat-top with limited voltage-second (Vs) of center solenoid (CS) coils is one of the most challenges of EHL-2. In order to minimize the consumption of Vs, fully non-inductive start-up by ECRH will be applied in EHL-2. The ramp-up phase will be accomplished with the synergetic mode between CS and non-inductive methods. The strategy of non-inductive start-up and ramp-up with synergetic mode has been verified on EXL-50U's experiments. Based on this strategy, numerical simulations give the feasibility of EHL-2 to achieve 3 MA plasma current. A high-performance steady-state scenario with I_p ~ 1.5 MA is also designed. In this scenario, the bootstrap current fraction f_{BS} > 70%, the safety factor q at the magnetic axis q_0 > 2, the minimum safety factor q_{min} > 1, the poloidal beta β_p > 3 and normalized beta β_N > 2.3. Each design iteration integrates the validation of physical models with the constraints of engineering implementation, gradually optimizing the performance of the heating and current drive (H&CD) systems. Numerical simulation results for general auxiliary H&CD systems such as neutral beam injection, electron cyclotron wave, ion cyclotron wave, and lower hybrid wave are presented. These simulation results ensure that the 31 MW H&CD systems comprehensively cover all scenarios while maintaining engineering feasibility.

Keywords: spherical torus, EHL-2, scenario, heating and current drive

(Some figures may appear in colour only in the online journal)

1 Introduction

Spherical torus (ST), known for their high β (the ratio of plasma pressure to magnetic field pressure) properties and compact structure, hold significant potential in fusion research [1, 2]. ENN Science and Technology Development Co., Ltd., (ENN) has been working on ST research for many years and has built the ENN XuanLong-50/50 Upgrade (EXL-50/50U) [3–5]. Based on 50 GHz electron cyclotron (EC) heating & current drive (H&CD), 1.1 voltage-second (Vs) central solenoid (CS) and 30 keV @ 0.5 MW neutral beam injection (NBI), the successful experimental results of the EXL-50U include: ion temperature T_i ~ 1 keV , plasma current I_p ~ 500 kA and center electron density $n_{e0} \sim 2 \times 10^{19}$ m^{-3} [6]. EXL-50U played a crucial role in supporting the construction of ENN He Long-2 (EHL-2) ST, which is an essential device on the path to p-^{11}B fusion [6]. The preliminary design parameters for EHL-2 can be found in table 1 [7].

Table 1. The preliminary target parameters for ENN EHL-2 ST.

Parameters	Values
Plasma current I_p (MA)	~3.0
Magnetic field B_0 (T)	~3.0
Beta β	0.11
Confinement time τ_E (s)	0.5
Major radius R_0 (m)	1.05
Aspect ratio A	1.85
Average/peak density n_e (m^{-3})	-/1.3×10^{20}
Heating power P_{heat} (MW)	31
Average/peak ion temperature T_i (keV)	-/30
Hot ion mode T_i/T_e	3

To ensure that the design of EHL-2 meets both physical and engineering requirements, an iterative design approach has been adopted. From an engineering and temporal perspective, we first confirm the CS material, the toroidal field (TF) coils' engineering capability, and the full device size chain. The EHL-2 device size chain has been finalized but is constrained by the materials required for the device and the compact ST specificities [8]. These specificities include a CS with a capacity

of 5 Vs. When considering the auxiliary heating systems and vacuum vessel windows, it is necessary to iteratively refine the space requirements and positioning of the auxiliary H&CD systems, such as the NBI and radio frequency (RF) systems.

This paper is organized as follows. Section 2 presents the strategic solutions to address the challenges of EHL-2. Section 3 outlines the predict operational scenario, while section 4 elaborates on the H&CD configurations and their role in scenario, including NBI, EC, Ion Cyclotron Wave (ICW) and Low Hybrid Wave (LHW). Section 5 is a summary. Through a process of detailed design segmentation and iterative optimization, a comprehensive and scientific framework has been developed for the final H&CD design of EHL-2. This framework guides the non-inductive start-up, ramp-up and flat-top phases, ensuring device reliability and performance. Our ENN team aims to achieve predetermined objectives in an optimized operating scenario.

2 Challenge and strategy for H&CD in EHL-2

Early identification and resolution of technical challenges are critical to the ENN developmental trajectory. The EHL-2 current evolution scenario strategy is given in figure 1.

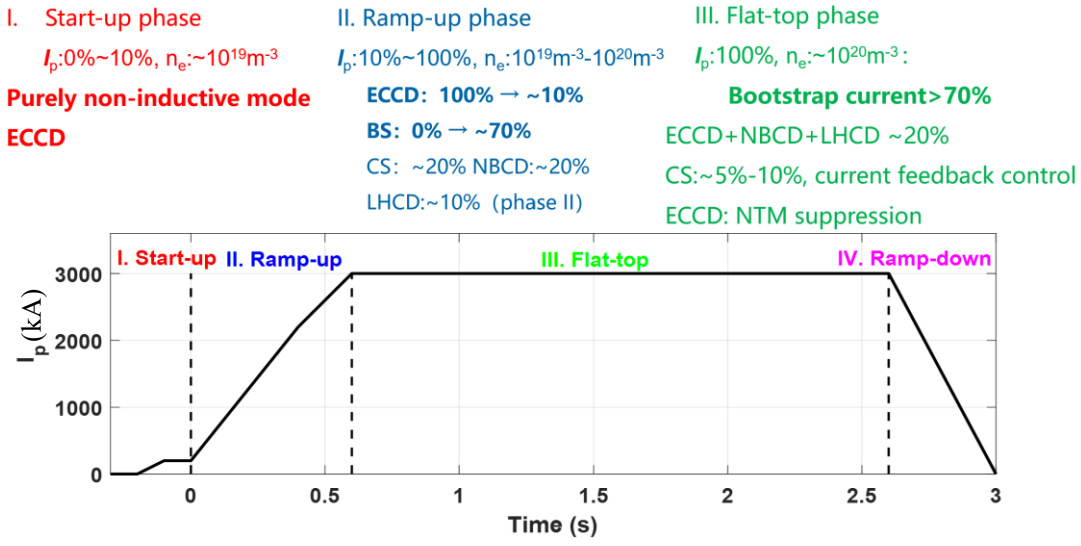

Figure 1. The EHL-2 current evolution scenario strategy.

In the start-up phase, pure EC is used for non-inductive start-up to achieve 0%–10% of the plasma current. Then, during the ramp-up phase (current rises from 10% or 20% to 100%), the CS is activated while the bootstrap current increases. NBI can also be added during this phase. Finally, the flat-top phase is maintained by the bootstrap current, with the CS used for feedback control, and EC along with NBI providing the remaining non-inductive contribution. By exploring the strategy illustrated in figure 1, we can identify the primary H&CD challenges, which include:

•Central solenoid operation

There are several challenges faced in a magnetic confinement machine with the CS, particularly in achieving an optimal current ramp-up rate and managing the limitations of Vs capacity. NSTX has reached their highest plasma current with a ramp-up rate of 5 MA/s [9], while DIII-D and JET operate with lower ramp-up rates of 1.2–2 MA/s and 2–3 MA/s in different ways [10, 11], respectively, to maintain stable flat-top phase and longer pulse durations. However, these differences in ramp-up rates and CS Vs capacities highlight the difficulties in achieving the desired performance across different devices. The low aspect ratio in ST further limits the space available for the CS in the central column, constraining the available Vs and complicating the control of inductive currents, particularly with superconducting coils that cannot match the rapid current changes of conventional copper coils. Future ST devices transitioning from copper to superconducting CS coils will require careful management of the loop voltage during breakdown, as well as consideration of ohmic saturation and feedback control in experiments.

•Verification of non-inductive current drive techniques

When the CS Vs is exhausted, validating non-inductive current drive methods, including Neutral Beam Current Drive (NBCD), Electron Cyclotron Current Drive (ECCD), and Lower Hybrid

Current Drive (LHCD), is key to achieving sustainable and economical compact fusion reactor. The elimination of the need for an ohmic heating solenoid may be the most impactful design driver for the realization of economical compact fusion reactor systems [12]. The realization of this idea also creates new requirements for auxiliary H&CD systems. Shear reversal, neoclassical tearing mode (NTM) stabilization and edge localized mode control are among the goals of EAST EC system [13]. It should be noted that ECCD has not been tested on the largest high-performing STs yet and is mainly studied in small devices [14]. Therefore, the effectiveness of non-inductive current drive to improve plasma current control in ST needs to be demonstrated experimentally, not only in the start-up phase, but also in the flat-top phase. Across all ECW experimental data from EXL-50, the average ECCD efficiency is approximately 1 A/W, which is double the efficiency observed in comparable international devices [15, 16]. Specifically, the EXL-50U device has now achieved 500 kA plasma current by using 50 GHz ECW + CS. How to sustain plasma current without CS is still underway.

2.1 EXL-50&50U extrapolation

Extrapolating data from the EXL-50 and EXL-50U devices provides base support for developing the EHL-2 operational scenario. These estimates form a foundation for subsequent design and optimization processes [3, 5, 16, 17].

The EXL-50 experiment demonstrates the high efficiency of non-inductive current drive, while the EXL-50U experiment further confirms that, under non-inductive start-up conditions, the integration of the CS significantly reduces the Vs consumption of the CS as figure 2 shows.

The tokamak simulation code (TSC) [18] enables the coordinated use of CS, EC and NBI during the ramp-up phase. TSC is a sophisticated numerical model specifically designed to simulate the evolution of axisymmetric tokamaks. This comprehensive tool has been extensively utilized not

only to replicate normal discharges in established magnetic confinement fusion devices such as TFTR [18], QUEST [19], and EAST [20], but also to provide predictive insights into future experimental scenarios in ITER [21].

For modeling the ohmic discharge of EXL-50U, the initial plasma equilibrium is calculated based on the specified coil currents and plasma parameters at that moment. Following this, the equilibrium evolves over time. The initial plasma parameters include the plasma current start at 80 kA, plasma line-averaged electron density reached 3×10^{19} m^{-3} at 250 ms, up from the initial 1×10^{19} m^{-3}, toroidal magnetic field 0.9 T, effective charge of plasma Z_{eff} = 2.5.

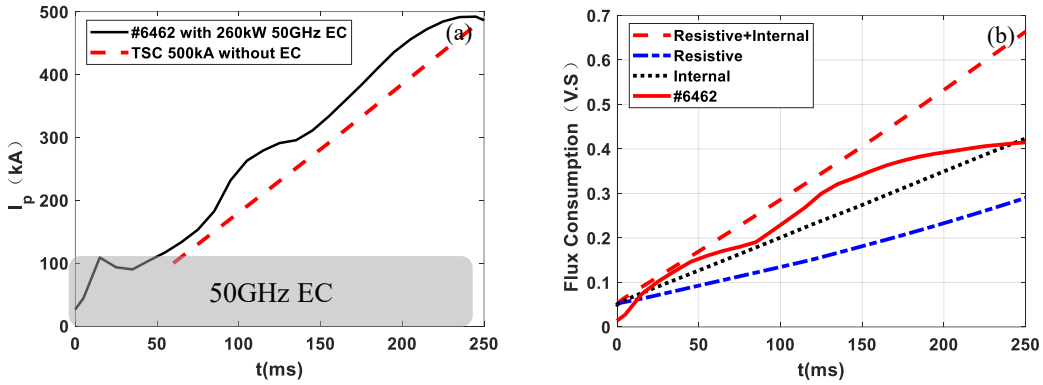

Figure 2. EXL-50U #6462 experiment & TSC 500 kA simulation. (a) Time evolution of I_p in ramp-up phase, black line is #6462 (EC + Ohm) experiment data and red one is TSC result without EC. (b) Flux consumption, blue dash-dotted line: resistive Vs consumption to sustain the ohmic dissipation; black dotted line: internal Vs consumption; red dashed line: resistive add internal contribution; red line: #6462 experiment flux consumption.

In experiment #6462, 50 GHz ECW is used for the initial plasma breakdown and later combined with the CS during the ramp-up phase, as shown in figure 2(a). As indicated by the red dashed line, the TSC simulation uses pure ohmic heating throughout the process. Both methods enable a 500 kA current to be driven within 0–250 ms. With reference to MAST, we consider the pure ohmic breakdown and CS consumption for the 0–80 kA segment to be 0.05 Vs [22]. In figure 2(b), the flux consumption in the simulation from 80 kA to 500 kA of plasma current is 0.65 Vs,

exceeding the 0.4 Vs consumed in experiment #6462, where ECW was used. This demonstrates that EC saves Vs required for breakdown and partial current ramp-up. In J-TEXT experiment, this hybrid approach is designed to leverage the advantages of EC waves in reducing the initial Vs consumption of the CS. The E_{min} in start-up phase, supplemented by ECW, is 29% compared to the pure Ohm start in J-TEXT. At t = 10 ms before, the Vs consumption of ECW-assisted starting is 16% of that of Ohm start. The plasma current of ECW-assisted starting is 36% of that of ohmic start [23]. By effectively using 28/50 GHz ECW during the start-up phase, a significant amount of Vs can be conserved. This reduction is essential for enabling longer plasma discharges and improving the overall efficiency of the current drive system.

These simulations were iteratively refined to ensure robustness and reliability in achieving the desired plasma performance. By utilizing foundational data from the EXL-50U experiment in combination with simulations, we can develop a plasma current scenario strategy to help overcome two challenges associated with EHL-2.

3 Operating scenario and conditions

This section provides an overview of the operating scenarios, focusing on two key areas: the first outlines the methodology for achieving a 3 MA plasma current, while the second details the strategies for maintaining the current to establish and sustain a high-performance steady-state scenario.

3.1 High plasma current target-3 MA

Insights from the EXL-50/50U experimental results show that the EC or EC with CS could both achieve a plasma current of 200 kA. The next stage is current ramp-up phase, which needs to consider the ramp rate and Vs consumption. Through discharge simulation parameters for the EHL-

2 [24], the initial plasma parameters include the plasma current start at 200 kA, plasma line-averaged electron density reached 1×10^{20} m^{-3} at 2800 ms, up from the initial 8×10^{18} m^{-3}, toroidal magnetic field 3.0 T, and Z_{eff} = 2.5. The results of pure ohmic current drive are shown in figure 3, which illustrates a detailed breakdown of the Vs consumption using the Poynting method [25]. Preliminary estimates suggest that with a ramp rate of 1 MA/s, the ohmic ramp-up process to 3 MA results in a total voltage consumption of 5.4 Vs.

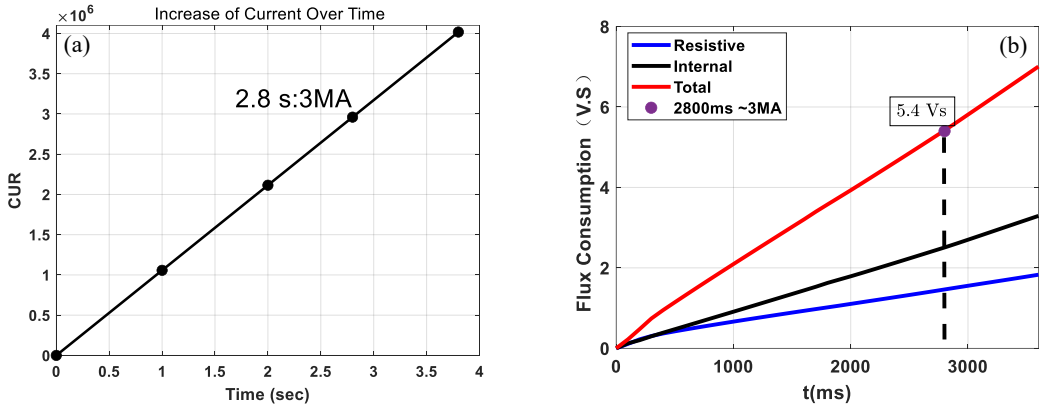

Figure 3. (a) 1 MA/s ramp-up rate to 4 MA current. (b) 5.4 Vs consumption at t = 2800 ms, total flux consumption includes resistive, internal and other Vs consumption.

However, both the ramp rate and the magnetic flux exceed EHL-2 engineering limits. Considering the constraints imposed by the TF and CS, the TF can only provide a 3 T toroidal magnetic field for less than 3 s, and the CS can only offer a single-sided Vs capacity of 2.4 Vs, with a maximum turn current of 35 kA. The magnetic material and heat generation of the CS coil limit us to only 5 Vs. Beginning with plasma current of 0.2 MA, the ramp-up to 3 MA over 2.8 s leads to a total Vs consumption of over 5.4 Vs, which is completely unacceptable. Furthermore, it is important to note that this calculation excludes the Vs consumption associated with the initial plasma breakdown and the ramp-up to 0.2 MA.

Using earlier plasma shaping at lower plasma currents is advantageous for reducing overall Vs consumption [26]. The synergetic mode inclusion of 105 GHz @ 6 MW EC and 60 keV @ 4 MW

NBI systems is shown in figure 4 to reduce the Vs consumption. The use of EC and NBI in the ramp-up phase allows the plasma to reach 2 MA at 1.72 Vs consumption and a current ramp rate of 3 MA/s. Without H&CD, it takes 3.7 Vs to reach and sustain 2 MA at a ramp rate of 3 MA/s using pure Ohm. The R_0 = 1.15 m, a = 0.53 m, the elongation ratio (k) is 2.26, and the electron central plasma density is 0.67×10^{20} m^{-3}.

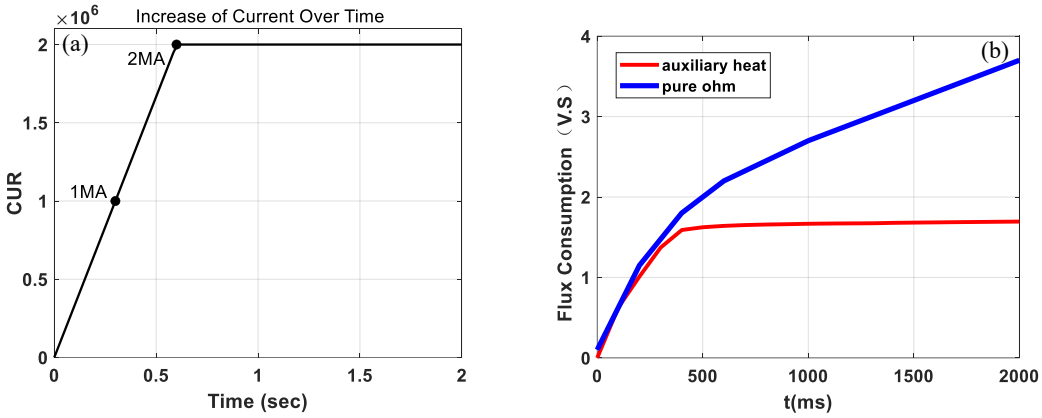

Figure 4. (a) 3 MA/s ramp-up to 2 MA current. (b) Vs consumption simulation results, red curve is the use of anxiliary heating systems: 6 MW @ 105 GHz EC and 4 MW @ 60 keV NBI, blue curve is the use of pure Ohm.

The plasma current is initially driven using a combination of partial ohm heating. Subsequently, NBI feedback is introduced to increase plasma temperature, density, and pressure gradient, thereby enhancing the share of bootstrap current [27]. Figure 4 shows that a 3 MA/s ramp rate can reach 2 MA, and in figure 5, further optimization of the ramp-up rate is demonstrated by adopting a two phases current ramp, from 0.2 MA to 2 MA in 40–400 ms, followed by EC and NBI injection from 400 ms to 600 ms. The average ramp-up speed of 5 MA/s is considered.

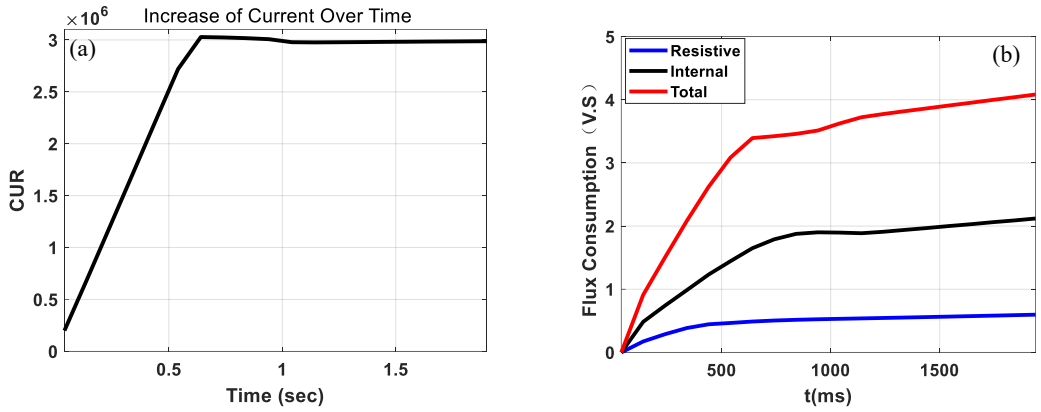

Figure 5. Average ramp-up rate of 5 MA/s to 3 MA. (a) Plasma current ramp-up phase. (b) Vs consumption simulation results, anxiliary heating systems: 6 MW @ 105 GHz EC and 4 MW @ 60 keV NBI.

By optimizing injection timing with segmented ramps and auxiliary heating, the high plasma current target can be achieved. The goal is to increase the average current ramp rate to 5 MA/s to reach the 3 MA plasma level, and it takes 3.4 Vs at 600 ms. In the flat-top phase, the total cost is 4.1 Vs in 2000 ms, with approximately 1 Vs remaining, and the results meet both the engineering requirements and the physical conditions for this phase.

3.2 High-performance steady-state scenario

Another objective for the EHL-2 is to achieve and maintain a high-performance steady-state operation mode using non-inductive current drive. In such a steady-state scenario, where plasma current is sustained by non-inductive means, the self-generated bootstrap current should contribute significantly to the plasma current, minimizing the reliance on external current drive systems. The ability to maintain such a steady-state operation is vital for future fusion reactors, particularly hydrogen-boron fusion reactors, where long-duration operation is paramount.

In flat-top phase, figure 6 shows a possible operation scenario of EHL-2 explored and analyzed by using the 0.5D integrated simulation code METIS [24]. During the simulation, the main ion

species is hydrogen and boron-11 is considered as an impurity. The plasma effective charge Z_{eff} is set to 2.5 for all locations, corresponding to 10% of boron-11. The density profile prediction here is based on three estimates: the density at the separatrix, the pedestal density and the density peaking factor. The density peaking is predicted by Weisen's scaling taking into account the collisionality dependence [28]. The thermal transport process is solved in two steps by separating the time and radial dimensions. The coefficients of heat transport follow the Bohm/gyro-Bohm model [29, 30]. The energy confinement time follows the size-dependent ST scaling law [31]. The bootstrap current and resistance are calculated by the Sauter formula (1D) [32, 33].

The toroidal magnetic field B_T is fixed at 2 T in this study due to the challenges of sustaining the TF magnetic field at 3 T conditions. Plasma current varied between 1 MA and 1.5 MA. This range was chosen based on previous experimental data suggesting that currents in this range allow for non-inductive partial improvement (f_{ni} = 100%) without leading to excessive magnetohydrodynamic (MHD) instabilities. Density is a critical parameter, directly influencing the bootstrap current fraction and overall confinement [34]. In this study, we focus on a density range around (6–10)$\times 10^{19}$ m^{-3}. This density was selected based on its compatibility with the target q values ($q_0 > 2$, $q_{min} > 1$) and the need to maintain a high bootstrap current fraction ($f_{BS} > 70\%$) while avoiding excessive NTM. We aim for q_{95} in the range of 10–40 to balance current drive efficiency with the avoidance of MHD instabilities [14]. The operating conditions are also optimized for a normalized beta (β_N) larger than 2.3 and poloidal beta (β_p) larger than 3, indicative of good confinement and stability performance. Other parameters, such as plasma rotation (v_r ~ 100–300 km/s) and H&CD system (NBI, EC), are optimized for a reasonable power level.

In high-performance steady-state scenarios, optimizing the reversed shear profile can further

improve plasma confinement and stability. Estimates using METIS suggest that a high-performance steady-state operational mode can be achieved with the application of 6 MW @ 80 keV NBI and 4 MW @ 105 GHz EC power with a deposition location at a normalized minor radius $\rho \sim 0.4$. In this simulation, two NBI systems with different powers and injection energies are implemented at 1 s. The major radius R_0 of plasma here is 1.05 m.

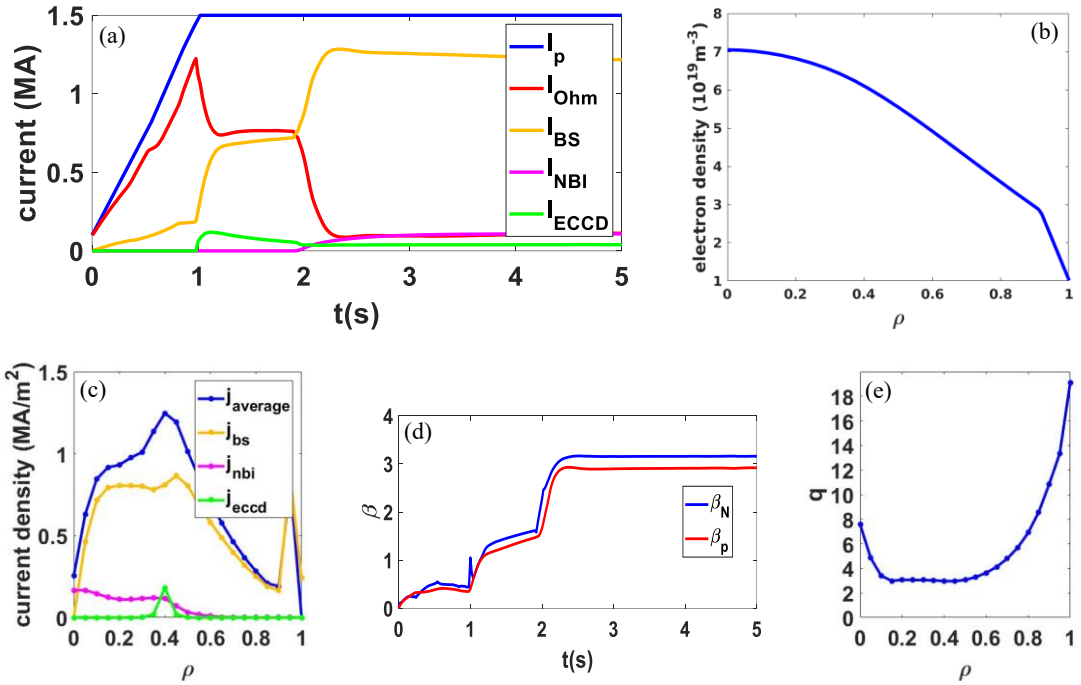

Figure 6. High-performance steady-state operation. (a) Auxiliary heating, (b) plasma current, (c) the density profile, (d) β, (e) the q profile at $t = 5$ s.

A possible high-performance steady-state operation scenario predicted by METIS is shown in figure 6. In this case, the target central density is set to 7×10^{19} m^{-3}. In the flat-top phase, the bootstrap current fraction accounts for 81.1%, the ohmic current fraction accounts for 7.5%, the total NBCD fraction accounts for 7.2%, and the ECCD fraction accounts for 2.6%. The loop voltage is 0.02 V. The profile distribution of different parameters at $t = 5$ s during the steady phase. T_i at the center is 14 keV, T_e is 8 keV. β_N and β_p are greater than 3. $q_0 = 9.1$, $q_{min} > 1$, with $q_{95} = 14.4$, indicating a reverse shear profile. This simulation case meets the target parameters with a bootstrap current

fraction (f_{BS}) greater than 70%, q_0 greater than 1.5, q_{min} greater than 1, and q_{95} greater than 5, β_N larger than 2.3 and β_p larger than 3.

The CRONOS code predicts the behavior of plasma by solving the current diffusion equation, transport equations for heat and particles, and the rotation equation. It features a highly modular structure that allows for the calculation of various physical processes, with the flexibility to alter the selection of modules based on simulation requirements. In its application to the high-performance steady-state operation mode of EHL-2, CRONOS employs 2D equilibrium calculation module (HELENA), neoclassical transport module (NCLASS), source module (SINBAD+REMA), and turbulence transport model (GLF23) [35, 36]. CRONOS can inherit the simulation parameters of METIS for calculation. Rotation is not added to CRONOS, and there are also differences between the two transport models, resulting in a certain temperature gap. More analyses of the effect of transport models on temperatures using ASTRA are discussed in the same series of articles [37].

This section is more concerned with the implementation of high-performance steady-state operation mode. A suitable electron density condition allows better control of the EC current deposition profile. Both β_N and β_p need to be considered at the same time. The core electron density n_{e0} is controlled at 7×10^{19} m^{-3}. A simulation is shown in figure 7.

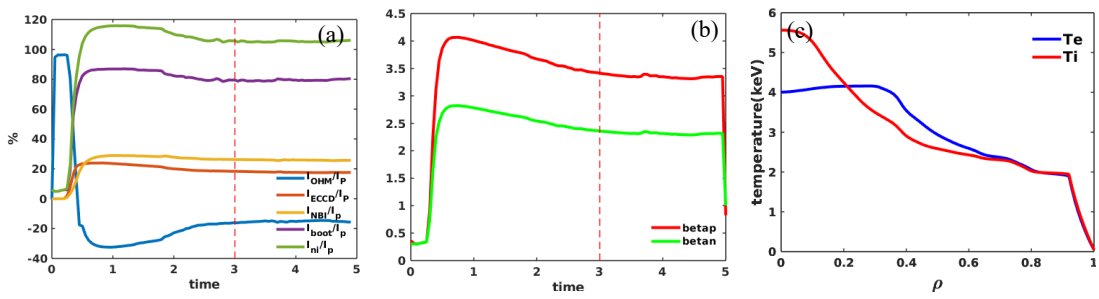

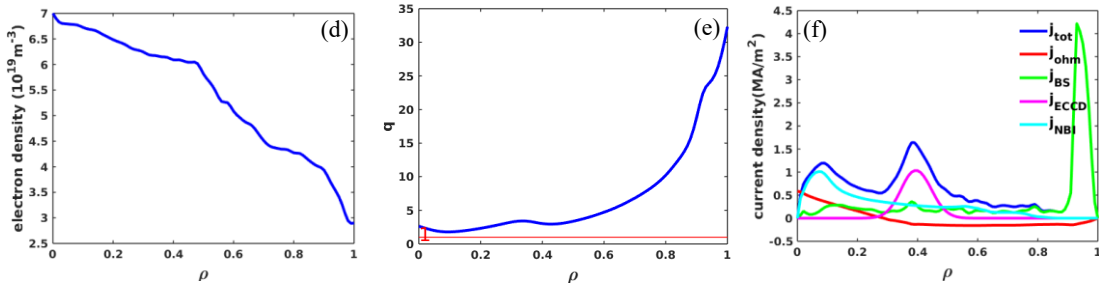

Figure 7. 1.5 MA fully non-inductive current mode simulation, the steady-state data from t = 3 s (red dashed line in (b)). (a) Evolutions of f_{NBI}, f_{boot} (f_{BS}) and f_{ni}, the f_{ni} reached 105.7%. (b) Evolutions of β_{p} and β_{N}, in which β_{p} reached 3.41 and β_{N} reached 2.36. (c) The ion temperature and electron temperature profiles, the core temperature T_{i0} and T_{e0} are 5.57 keV and 4 keV. (d) The election density profile, the core density n_{e0} is 7×10^{19} m^{-3}. (e) Safety factor q. (f) Current density profiles, the distributions of j_{tot}, j_{ohm}, j_{BS}, j_{ECCD} and j_{NBI} are shown.

Under the current heating conditions, when reaching a steady-state (t = 3 s), the core T_{i} reaches 5.57 keV, and T_{e} reaches 4 keV, forming a 2 keV temperature pedestal. The peak power of NBI occurs at the position of ρ = 0.05, providing heating powers of 1.8 MW · m^{-2} for ions and 0.86 MW · m^{-2} for electrons. ECW is set in off-axis, with the driving peak set at the position of ρ = 0.4, generating a heating power of 3.05 MW · m^{-2} for electrons, forming a weak magnetic shear profile, with q_{95} = 24.4, q_0 = 2.5, and q_{min} = 1.78. The bootstrap current is mainly present at the edge, with a share of f_{BS} reaching 79.5%. The poloidal beta β_{p} is 3.41, and the normalized beta β_{N} is 2.36, achieving lower ion core transport.

Table 2. METI&CRONOS simulation parameters.

H&CD system	**Parameters**	**Power (MW)**
NBI	60 kV	4(CRONOS)
	80 kV	6(METIS)/4(CRONOS)
EC	105 GHz	4(METIS)/6(CRONOS)

Current simulation outcomes from METIS and CRONOS indicate that by using the H&CD parameters from table 2, at a plasma current of 1–1.5 MA and a magnetic field of 2 T, it is feasible to achieve a high-performance steady-state scenario. This scenario meets the requirements: f_{BS} exceeds 70%, and q_0 is greater than 2, q_{min} is above 1, q_{95} in the range of 10–40 and β_{p} exceeds 3,

β_N greater than 2.3. Eventually, the f_{ni} can be increased to approximately 100% in the flat-top phase. METIS and CRONOS, incorporating current profiles generated by the GENRAY/CQL3D [38, 39] and NUBEAM [40] codes, were employed to fine-tune and optimize these scenarios.

4 Heating system requirements and arrangement in EHL-2

Based on the experimental parameters from EXL-50/50U, estimates indicate that approximately 17 MW of heating is required. Physically, it is crucial to understand the characteristics of the NBI, EC, and other systems, as shown in figure 8.

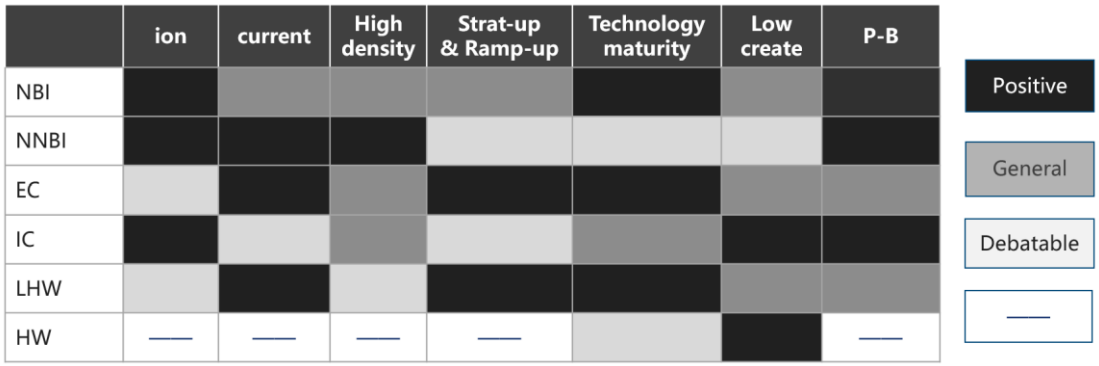

Figure 8. H&CD system role judgment and comparison of different plasma heating and current drive methods. NBI – Neutral Beam Injection; NNBI – Negative ion source Neutral Beam Injection; EC – Electron Cyclotron; IC – Ion Cyclotron; LHW – Lower Hybrid Wave; HW – Helicon wave (High Harmonic Fast Wave).

The grayscale intensity in figure 8 represents the maturity or effectiveness of different technologies across various dimensions. Darker shades (closer to black) indicate higher maturity or better performance, suggesting that these technologies are more advanced or efficient in that particular category. Lighter shades (closer to white) represent lower maturity or poorer performance, implying these areas may require further development or optimization. In our H&CD system role judgement, NBI and negative ion source neutral beam injection (NNBI) source must first be developed to address long-cycle engineering challenges, its benefit to ion heating and current drive in high density. Due to the maturity of the EC system technology and its ability to function in all

discharge processes, EC is also essential. Through a combination of simulation and iterative optimization, the NBI, EC, and other systems are tailored in table 3 to overcome the challenges posed by the EHL-2 design.

Table 3. Design of EHL-2 heating parameters.

H&CD system	EHL-2 parameters	Total power (MW)	Pulse length (s)
NBI	1×4 MW @ 60 kV	17	5
	2×5 MW @ (80–100) kV		5
N-NBI	1×3 MW @ 200 kV		5
EC	1×1 MW @ 50 GHz	7	5
	6×1 MW @ 105&140 GHz (dual frequency)		5
IC (Phase II)	5 MW @ 30–75 MHz	5	5
LHW (Phase II)	2 MW @ 2.45–5 GHz	2	5

4.1 Neutral beam injection

The simulation parameters for the NBI system have undergone multiple iterations, initially focusing on optimizing beam energy, tangential injection radius, and beam power. EHL-2 NBI beam energy has been scanned. As shown in figure 9, the average electron density is 6×10^{19} m^{-3}. This is under the conditions where both the central electron/ion temperature and electron density follow a classical parabolic profile. The center ion temperature is set to 20 keV and center electron temperature is set to 14 keV, with increasing injected beam energy and beam power, the shine-through loss increases and the heating of ions and electrons decreases. Because the temperature is set higher, there is a certain share of themalization loss.

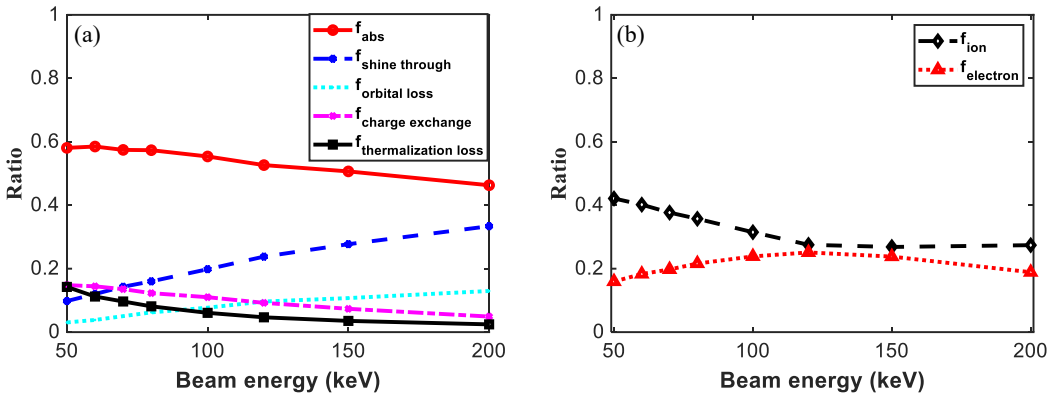

Figure 9. (a) EHL-2 NBI beam scan. f_{abs}: fraction of NBI totally absorb, $f_{shine\ through}$: fraction of beam shine-through loss, $f_{orbital\ loss}$: fraction of NBI orbital loss, $f_{charge\ exchange}$: fraction of NBI charge exchange loss, $f_{themalization\ loss}$: fraction of NBI themalization loss. (b) Fraction of ion heating and electron heating.

Then, the energy of the injected neutral beam is set at 50 keV. The plasma current is set to 3 MA. As the electron density increases, the shine-through losses decrease significantly, leading to an increase in the share of ion and electron heating. This situation is found in EAST, J-TEXT [41], the capture and slowing down of the beam are mainly through the classical collision with the plasma (including charge exchange), and no obvious abnormal slowing down process is found. The total efficiency of neutral beam heating can be more than 90%, which is a effective heating method [42]. We changed the density distribution as shown in figure 10(a) and set the electron temperature to 2 keV as shown in figure 10(b). The average string density is set at 7×10^{19} m^{-3}, the center density is 12×10^{19} m^{-3}, and the product of the longitudinal field and the large radius is 3.15 T • m. Given the advantages of the ST configuration, tangential injection is particularly beneficial. The major radius R = 1.05 m. At different tangency radii shown in figure 10(c), by scanning the tangency radius of EHL-2 and through iterative optimization, the left beam tangency radius is set to 75 cm and the right beam tangency radius to 88 cm. Both beams can inject ~ 90% of the power when combined with the plasma, with ion heating being the major part.

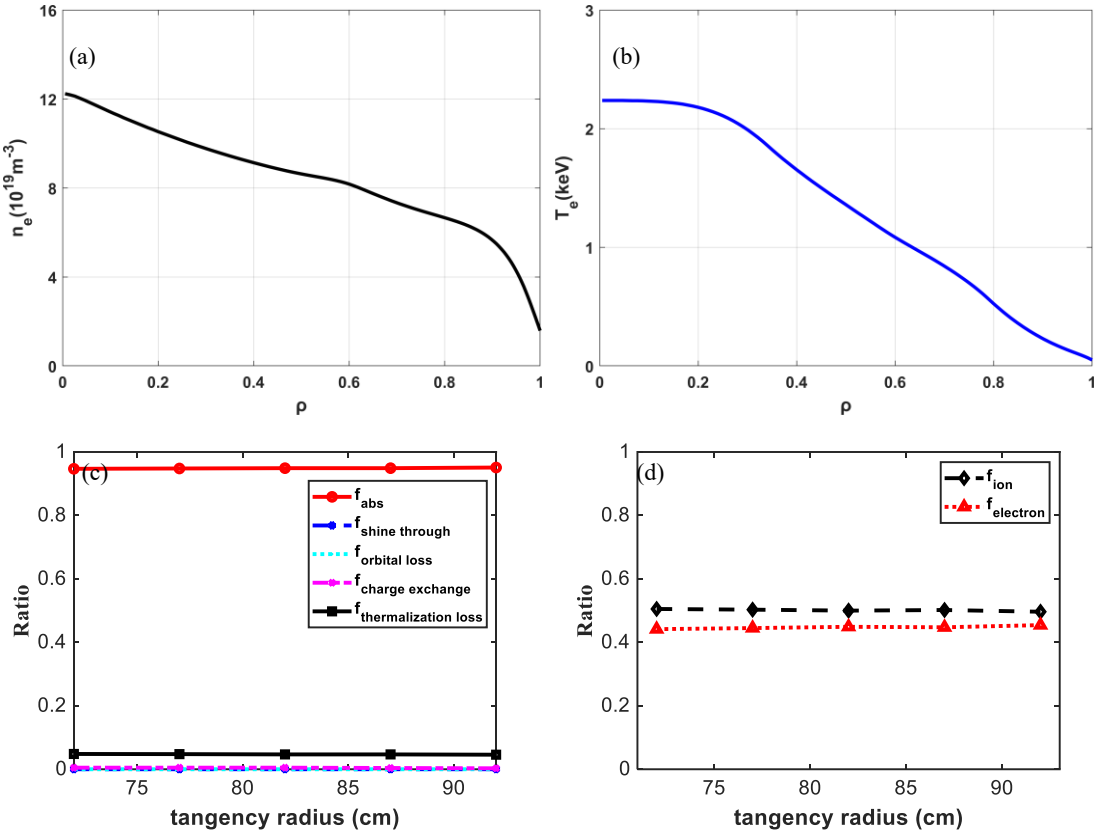

Figure 10. EHL-2 NBI tangency radius simulation. (a) Density profile. (b) Electron temperature profile. (c) Tangency radius scan. (d) Absortion from ion and electron.

Consider about optimum neutralisation efficiency for different positive and negative hydrogen ion species against beam energy per nucleon [43], and the design parameter should be greater than simulation to handle unpredictable situation. Beam energy is selected as 60 keV for heating low-density plasmas, 80–100 keV for H^+ neutralization parameters to limit, and 200 keV for developing hydrogen-boron (H-^{11}B) fusion reactions [44].

Parameters are refined to balance current drive efficiency and practical engineering constraints, ensuring the system's effectiveness and reliability in sustained plasma operation. Form the shown in figure 10(a), the beam-driven current density for the 80 keV left beampeaks at approximately J_{NBCD} = 35 A/cm^2. The profile exhibits a characteristic structure where the current density initially

rises sharply near the core region, reaches its maximum at ρ = 0.17, and subsequently decreases monotonically until around ρ = 0.4. Beyond ρ = 0.4, a secondary rise in J_{NBCD} is observed, forming a local maximum at approximately ρ = 0.5, before tapering off significantly towards the edge of the plasma. This distribution is consistent with the physics of a NBCD in a ST that can pass through a long plasma region where the deposition and synthesis current drive efficiency is very sensitive to beam energy, pitch angle, and collision. From the figure 10(b), it can be observed that the right beam exhibits a broader current density distribution compared to the left beam. This broadening leads to a more extensive coverage of the plasma cross-section and crosses the magnetic axis. Near the magnetic axis ($\rho \approx 0.1$), the beam-driven current density reaches a higher value J_{NBCD} = 45 A/cm^2 and maintains relatively high current density over a wider range of ρ.

Additionally, the design must account for practical engineering considerations, such as the arrangement of the beamlines and the positioning of the vacuum chamber windows. These factors determine the achievable beam-cut radius and are critical when considering both vertical and tangential injection schemes. This involves carefully selecting the number of beams, their energy levels, and their intervals, with a focus on maximizing power absorption while minimizing losses. The design scheme is shown in figures 10(c) and (d).

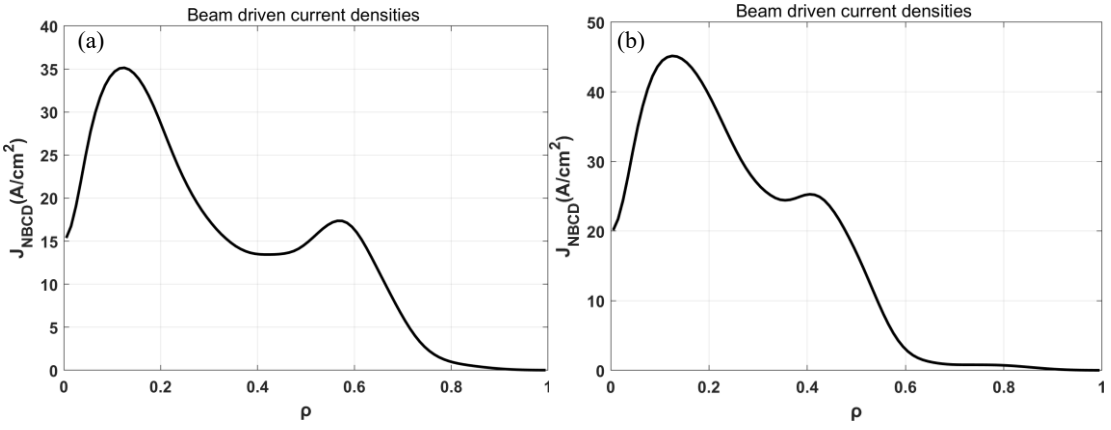

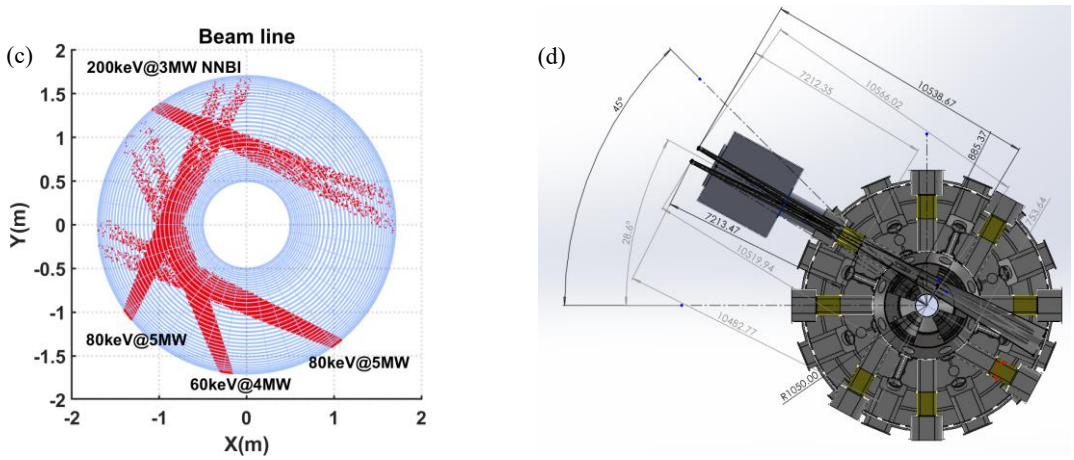

Figure 10. EHL-2 NBI beam line design. (a) 80 keV left beam driven current density, J_{NBCD} = 35 A/cm^2 peak in ρ = 0.17. (b) 80 keV right beam driven current density, J_{NBCD} = 45 A/cm^2 peak in ρ = 0.16. (c) All NBI beam lines inject partical show in plasma. (d) Design of EHL-2 NBI & vacuum windows.

4.2 Electron cyclotron heating system

In the EHL-2 device, the EC heating system is a critical component of the overall H&CD strategy. The choice of EC wave frequency and mode is essential for optimizing the performance of the EHL-2 system. Depending on the toroidal magnetic field strength, the final configuration confirms the use of 105/140 GHz dual-frequency. These frequencies are selected based on considerations of drive efficiency at both low and high plasma densities, as well as the available frequency windows.

Once closed magnetic surfaces are established, the asymmetric confinement of energetic electrons, which can reduce current, becomes less significant. Instead, the current generated by the directional wave vector within the closed magnetic surfaces, along with the bootstrap current driven by plasma pressure, becomes more prominent. This control ensures that the EC system effectively contributes to both the initial plasma breakdown and the sustained high-performance operation of EHL-2. In the EHL-2, the possibility of using the X-1 mode for efficient current drive with electron cyclotron waves (ECW) can be considered during the start-up phase. However, the density range that the X-1 mode can drive is limited, and the 105 GHz X2 mode has a density limit of $n_{\mathrm{ec,X,R}}$ =

6.83×10^{19} m^{-3}. This means that at higher plasma densities, the 105 GHz frequency may no longer provide effective current drive.

When the 105 GHz frequency is no longer effective, the injection of 140 GHz EC waves is recommended to sustain the ramp-up phase. By utilizing the characteristic steep magnetic field gradients in spherical torus, it is possible for both frequencies to operate with fundamental resonance layers within the closed magnetic surfaces. This enables sustained current drive under varying plasma density conditions.

Two primary heating options are considered:

- 105 GHz for conventional O-mode heating. This frequency is primarily used for fundamental heating, injected through an upper launch window. The effectiveness of this mode is evaluated based on its current drive efficiency across different toroidal and poloidal injection angles, as visualized in figure 11. This mode provides stable heating and current drive under lower-density conditions.

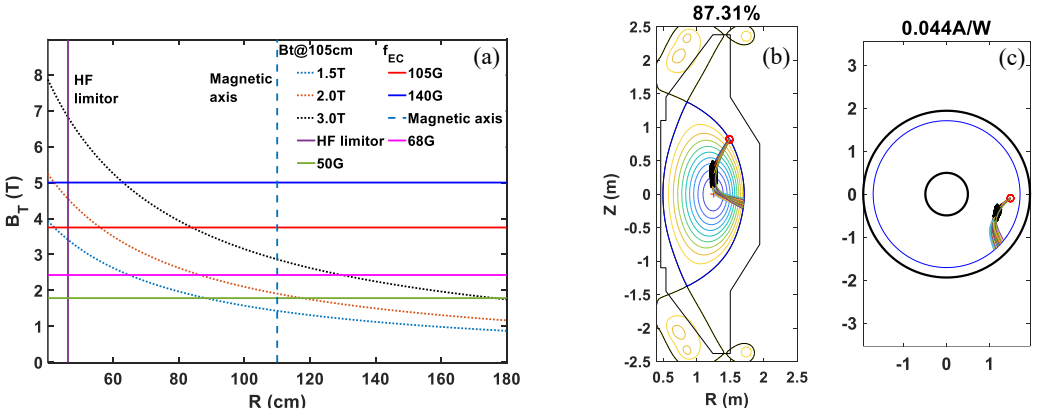

Figure 11. Toroidal magnetic field and 105 GHz. (a) The toroidal magnetic field B_t = 1.5 T, 2.0 T, 3.0 T. Green line – 50 GHz, pink line – 68 GHz, red line – 105 GHz, blue line – 140 GHz, $f = 28nB_t$, n is the number of harmonic frequencies. (b) Poloidal cross-section. (c) Toroidal cross-section and drive efficency $\eta = I_{cd}/P_{in}$ = 0.044 A/W. Black dots on the rays indicate power deposition. $n_{e0} = 6\times10^{19}$ m^{-3}, T_{e0} = 8.0 keV, f = 105 GHz, $(\alpha, \beta) = (204°, -50°)$.

- 140 GHz for X-mode second harmonic heating shown in figure 12. When the plasma density

exceeds the effective range of 105 GHz, 140 GHz X-mode heating becomes the preferred option. This higher frequency allows effective heating and current drive at higher densities, particularly beneficial during the ramp-up phase. The higher frequency is chosen for scenarios requiring enhanced heating capabilities.

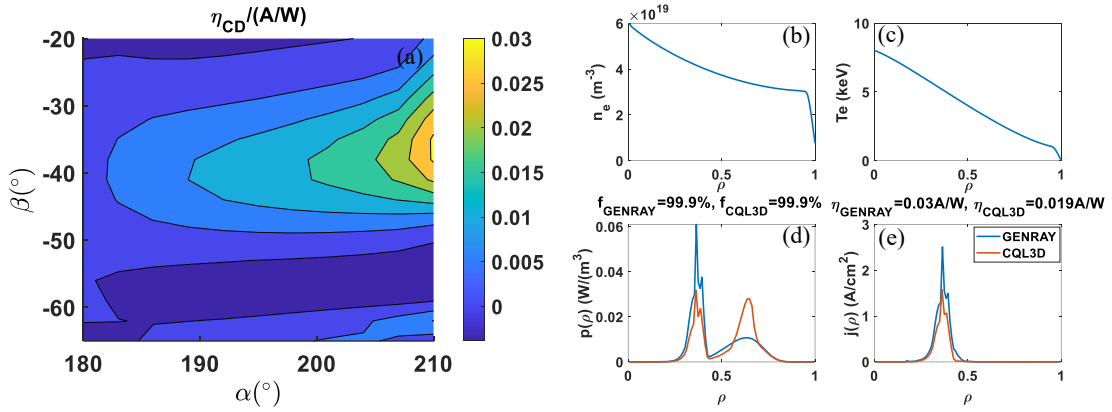

Figure 12. 140 GHz EC angle scan. (a) EC-driven current efficiency as a function of the poloidal angle α and toroidal angle β. (b) Radial profiles of electron density. (c) Radial profiles of electron temperature. (d) Power absorption radial profile calculated by GENRAY and CQL3D codes. (e) Driven current density profile calculated by GENRAY code, η = 0.03 A/W, and CQL3D code, η = 0.019 A/W.

The EC system in EHL-2 incorporates the mechanisms developed from EXL-50 & EXL-50U, such as higher harmonic resonance and multiple reflections, to enhance the efficiency of current drive. Consideration is given to the coordination of X-mode and O-mode EC waves to achieve plasma breakdown under different scenarios. The 50 GHz frequency is used for start-up and combined with 105/140 GHz dual-frequency ECW. This coordination enhances the flexibility of the EC system to adapt to varying plasma conditions. To further optimize the current drive, precise control over the EC wave beam and plasma parameters is required. A launch window will integrate four antennas to achieve this control. ECW are also employed to suppress NTM [45]. By strategically managing these modes, the EC system can meet the diverse experimental demands of EHL-2, ensuring its reliable operation under different scenarios.

4.3 Other H&CD systems

We have already discussed the specific physical considerations and engineering design of NBI and EC in EHL-2. ICW, LHW and other H&CD systems, are also being continuously explored in two aspects: physical synergy and engineering coupling. These systems will be included in the subsequent design phase, planned for the second stage.

4.3.1 Ion cyclotron (IC)

IC is one of the main heating methods in magnetic confinement fusion devices. It is considered to be installed in the second phase of EHL-2. This system is designed to meet the specific heating requirements necessary for achieving and sustaining high-performance plasma conditions. It will also play a role in promoting the p-^{11}B fusion rate due to the synergy effect with NBI. The IC system's contribution is particularly significant in scenarios where ion heating is critical to achieve the desired plasma temperatures and maintain overall stability. We also made a simple assessment of the space required for the IC system in the vacuum, as shown in figure 13.

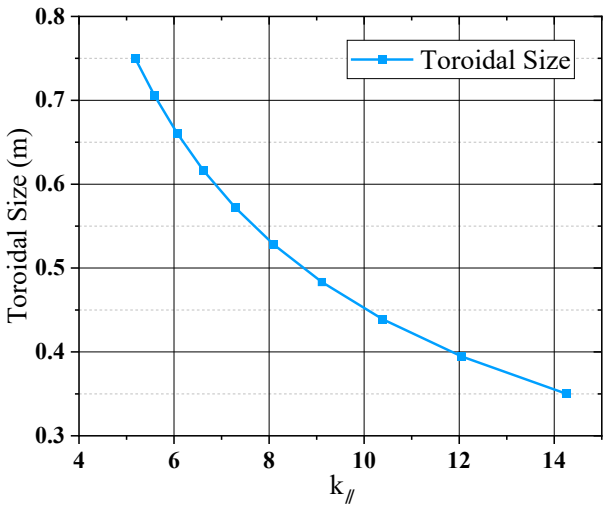

Figure 13. $k_{//}$ in different antenna toroidal sizes.

The heating mechanisms of the IC system will be determined from the following options:

fundamental frequency heating, second harmonic heating, minority heating, anomalous minority heating, and three-ion heating, etc. Since the ion cyclotron resonance heating (ICRH) operates within the ion cyclotron frequency range, attempts must be made to use second harmonic heating or minority heating. This will be the first attempt to apply ion cyclotron resonance heating to H-^{11}B plasma in a spherical torus and ensure that the IC system effectively complements with the NBI and EC systems [46, 47]. IC system parameters is shown in table 4.

Table 4. ENN ST IC heating parameters.

Parameter	For EXL50/50U	For EHL-2
Plasma density	1×10^{19} m^{-3}	1.3×10^{20} m^{-3}
Power	100 kW	4 MW
Magnetic field	0.9 T	3 T
Frequency	27 MHz	30–90 MHz
Number of antennas	2	2
Heating mode	Second harmonics	Second harmonics

4.3.2 Lower hybrid and helicon current drive

The wave trajectories of the 2.45 GHz LH waves for a mid-plane injection are shown in figure 14, in which the power absorption occurs at the points marked with black crosses. This simulation employs an injection power of 2 MW, resulting in a driven current exceeding 250 kA. The current drive profile, as indicated in the figure 14, is located at the periphery of the plasma, highlighting the specific impact and efficiency of the injection method used. As shown in figure 15, a possible candidate to LHCD, that is the helicon wave current drive (HWCD/HW), is also being considered, which may provide mid-radius current drive. However, the near-field coupling of LH and HW to the plasma and their parasitic parametric decay instability for high density discharge are two important issues, which require attention.

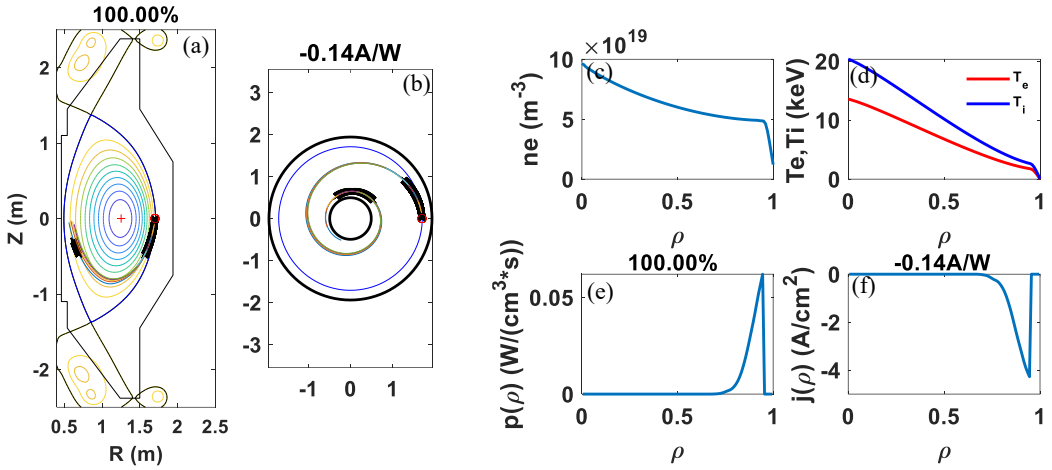

Figure 14. Simulation of 2.45 GHz ($N_{//} \sim 4$) LHCD mid launch. (a) Poloidal cross-section. (b) Toroidal cross-section and drive efficency $\eta = I_{cd}/P_{in} = 0.14$ A/W. (c) Radial profile of electron density. (d) Radial profiles of temperature. (e) Radial profile of power absorption calculated by GENRAY code. (f) Driven current density profile.

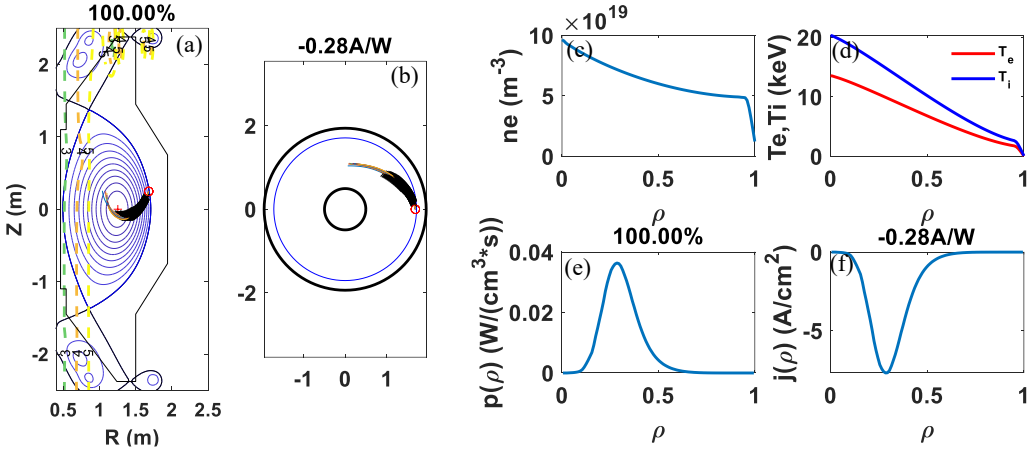

Figure 15. Simulation of 300 MHz ($N_{//} \sim 2.5$) helicon wave mid launch. (a) Poloidal cross-section. (b) Toroidal cross-section and drive efficency $\eta = I_{cd}/P_{in} = 0.28$ A/W. (c) Radial profile of electron density (d) Radial profiles of temperature. (e) Radial profile of power absorption calculated by GENRAY code. (f) Driven current density profile.

5 Discussion and future work

The challenges and solutions associated with the H&CD system in EHL-2 are explored through a meticulous examination of the engineering constraints and physical requirements. The iterative design methodology is applied in this study in addressing the unique challenges posed by EHL-2's compact structure, particularly the limited magnetic flux of CS. Therefore, non-inductive current

drive must play a key role in EHL-2.

Based on the achievements of current drive experiments in EXL-50 and EXL-50U, the main strategy for EHL-2's current drive is as follows. The start-up phase will be realized with fully non-inductive mode with ECRH. The synergetic mode between CS and RF or NBI will be applied in ramp-up phase. The numerical simulation analysis shows that the consumption of Vs is dramatically reduced with the application of RF or NBI in ramp-up phase. The simulation results show that EHL-2 can achieve a 3 MA plasma current with non-inductive fraction ratio of 50%. For the high-performance steady-state scenarios, 1.5 MA discharges are designed and the ratio of non-inductive current is about 80%.

By adjusting the auxiliary heating system, emphasis is placed on maximizing power absorption. The 17 MW NBI heating system was designed to minimize the power losses such as shine-through and orbital loss. The 7 MW ECW system will also participate in synergetic iterations of the simulation and ensure that the absorption is greater than 80% while maintaining current drive efficiency greater than 0.02 A/W. Wave-plasma coupling is being studied at ICW and LHW. This research has laid a strong foundation for achieving the desired plasma performance.

Acknowledgments

This work was supported by ENN Group and ENN Energy Research Institute. The authors would like to express their gratitude for the contributions of the ENN fusion team and collaborators, such as Tiantian Sub, Haojie Ma, and Yong Guo, in supporting these endeavours. The authors also acknowledge the support of the National SuperComputer Center in Tianjin and Beijing PARATERA Tech Corp., Ltd., for providing HPC resources that have contributed to the research results reported

in this paper.

References

[1] Peng Y-K M and Strickler D J 1986 *Nucl. Fusion* **26** 769
[2] Peng Y-K M 2000 *Phys. Plasmas* **7** 1681–92
[3] Shi Y *et al* 2022 *Nucl. Fusion* **62** 086047
[4] Wang M *et al* 2023 *J. Plasma Phys* **89** 905890603
[5] Banerjee D *et al* 2022 *J. Phys. Conf. Ser* **2397** 012011
[6] Shi Y *et al* 2024 submitted to *Plasma Science and Technology (EHL-2 special issue)*.
[7] Liang Y *et al* 2024 submitted to *Plasma Science and Technology (EHL-2 special issue)*.
[8] Liu M *et al* 2024 *Phys. Plasmas* **31** 062507
[9] Menard J E *et al* 2001 *Nucl. Fusion* **41** 1197
[10] Jackson G L *et al* 2010 *Fusion Sci. Technol.* **57** 27–40
[11] Sun H J *et al* 2023 *Plasma Phys. Control. Fusion* **65** 095009
[12] Ono M *et al* 2024 *Nucl. Fusion* **64** 086021
[13] Wang H *et al* 2023 *Plasma Sci. Technol.* **25** 025105
[14] Meyer H *et al* 2024 *Philos. Trans. R. Soc. Math. Phys. Eng. Sci.* **382** 20230406
[15] Chen B *et al* 2022 *Plasma Sci. Technol.* **24** 015104
[16] Wang M *et al* 2022 *Plasma Phys. Control. Fusion* **64** 075006
[17] Guo D *et al* 2022 *Plasma Phys. Control. Fusion* **64** 055009
[18] Jardin S C *et al* 1993 *Nucl. Fusion* **33** 371
[19] Kuroda K *et al* 2018 *Plasma Fusion Res.* **13** 3402059–3402059
[20] Li H *et al* 2014 *Nuclear Fusion and Plasma Physics* **34** 57–62
[21] Bandyopadhyay I *et al* 2010 Proc. 23rd Int. Conf. on Fusion Energy.
[22] Sykes A *et al* 2001 *Nucl. Fusion* **41** 1423–33
[23] Zhang J *et al* 2023 *Nucl. Fusion* **63** 076028
[24] Gu X *et al* 2024 submitted to *Plasma Science and Technology (EHL-2 special issue).*
[25] Ejima S *et al* 1982 *Nucl. Fusion* **22** 1313–9
[26] Liu C-Y *et al* 2020 *Chin. Phys. B* **29** 025202
[27] Huang J *et al* 2020 *Nucl. Fusion* **60** 126007
[28] Weisen H *et al* 2005 *Nucl. Fusion* **45** L1
[29] Erba M *et al* 1998 *Nucl. Fusion* **38** 1013
[30] Erba M *et al* 1997 *Plasma Phys. Control. Fusion* **39** 261
[31] Kaye S. M *et al* 2021 *Plasma Phys. Control. Fusion* **63** 123001
[32] Sauter O *et al* 2002 *Phys. Plasma* **9** 5140
[33] Sauter O, Angioni C and Lin-Liu Y.R 1999 *Phys. Plasma* **6** 2834
[34] Hou J *et al* 2024 *Results Phys.* **56** 107260
[35] Artaud J F *et al* 2010 *Nucl. Fusion* **50** 043001
[36] Houlberg W A *et al* 1997 *Phys. Plasmas* **4** 3230–42
[37] Wang X *et al* 2024 submitted to *Plasma Science and Technology (EHL-2 special issue).*
[38] Smirnov, A. P., and Harvey, R. W 1995 *Bull. Am. Phys. Soc* **40** 1837
[39] Harvey R W and McCoy M G 1992 *IAEA Technical Committee Meeting* 489-526
[40] Pankin A *et al* 2004 *Phys. Commun.* **159** 157–84

[41] Wu X *et al* 2013 *Plasma Sci. Technol.* **15** 480–4
[42] Sun T *et al* 2024 submitted to *Plasma Science and Technology (EHL-2 special issue)*.
[43] Speth E 1989 *Rep. Prog. Phys.* **52** 57–121
[44] Li Z *et al* 2024 submitted to *Plasma Science and Technology (EHL-2 special issue)*.
[45] Dong L *et al* 2024 submitted to *Plasma Science and Technology (EHL-2 special issue)*.
[46] Ma H *et al* 2024 *Plasma Sci. Technol.* **26** 025105
[47] Wu X *et al* 2024 *Plasma Sci. Technol.* **26** 104004